First-Principles Study on the Electronic Properties of PDPP-based Conjugated Polymer via Density Functional Theory

Amirhadi Alesadi[1], F Fatima[1], Wenjie Xia[1,2*], and Dmitri Kilin[3*]

[1]Department of Civil & Environmental Engineering, North Dakota State University, Fargo, ND 58108, United States

[2]Materials and Nanotechnology, North Dakota State University, Fargo, ND 58108, United States

[3]Department of Chemistry and Biochemistry, North Dakota State University, Fargo, ND 58108, United States

*To whom correspondence should be addressed.

Contact information:

dmitri.kilin@ndsu.edu

wenjie.xia@ndsu.edu

ABSTRACT

In this study, we focus on computational predictions of the electronic and optical properties of a one-dimensional periodic model of a single-chain of a diketopyrrolopyrrole (DPP) based conjugated polymer (PDPP3T) as a function of electronic configuration changes due to charge injection. We employ density functional theory (DFT) to explore the ground state and excited state electronic properties as well as optical properties influenced by charge injection. We utilize both the Heyd-Scuseria-Ernzerhof (HSE06) and Perdew-Burke-Ernzerhof (PBE) functionals to predict the band gap and compute the absorption spectrum. Our DFT results point out that utilizing the HSE06 functional in conjunction with momentum sampling over the Brillouin zone can appropriately predict band gap and absorption spectrum in good agreement with experimental data. Moreover, we explore the influence of charge-carrier injection on the electronic configuration of the PDPP3T polymer. Our results indicate that the injection of charge carriers into the PDPP3T semiconducting polymer model greatly affects the electrical properties and ended in a low bandgap and high-mobility of charge carriers in PDPP3T polymers, offering the potential to tailor the material electronic performance for organic photovoltaic and optoelectronic device applications.

Keywords: Conjugated polymers; Density functional theory; Hybrid functionals; Doping; *k*-point Sampling; Triplet state.

INTRODUCTION

Over the last decades, the development of donor-acceptor (D-A) type semiconducting conjugated polymers (CPs)[1–5] prompts considerable progress in organic electronic devices such as organic photovoltaics (OPVs) and field-effect transistors (OFETs).[6–10] It has been shown that CPs exhibit excellent solution processability, structural tenability, good optical and electrical properties as well as tunable mechanical compliance, compared to their inorganic counterpart silicon.[11–19] Among the CPs, diketopyrrolopyrrole (DPP)-based polymer (PDPP3T) has been increasingly utilized in the semiconductor industry due to its high charge mobility,[20] which makes it a promising material candidate in a wide range of applications such as flexible-wearable and biomedical devices. In particular, PDPP3T is known to show relatively high and balanced charge carrier mobilities for both electrons and holes accompanied by an extended optical absorption near the infrared (IR) region.[21] Despite considerable experimental and computational efforts, the ground state and influence of the injection of charge carriers on the electronic structure of this particular semiconducting polymer is less investigated at the atomistic level.

The charge carrier density and conductivity of semiconducting CPs can be modified via p- or n-type doping (charge injection).[22] Through the doping process (or injection of charge carriers), appropriate impurities with desired electronic properties can be added to donate an electron to the lowest unoccupied molecular orbital (LUMO) for n-type doping or to get rid of an electron from the highest occupied molecular orbital (HOMO) for p-type doping.[23,24] In the case of injection of the charge carriers, the polymer is not doped via chemicals; instead, the polymer is oxidized or reduced by adding or withdrawing electrons, respectively.[25,26] The applications of semiconductors in various devices can be expanded by tuning the energy of the band gap to achieve tailored performance.[27] For instance, in photovoltaic cells, a low band gap increases visible light absorption,

carrier mobility, and raises the photogenerated electron-hole pair separation.[28] Therefore, it is crucial to better understand the effect of charge injection on the electronic performance of CPs at a fundamental level. For this purpose, density functional theory (DFT), one of the most popular computational methods used in modern quantum-chemical modeling of materials, can be utilized to probe their fundamental electronic structures.[29,30] Besides the appropriate accuracy, computational costs of DFT calculations are relatively low compared to traditional methods, such as exchange only Hartree-Fock (HF) theory.

The Hohenberg-Kohn theorems[31] indicate that the ground state and properties of a many-electron system could be a unique functional of the electron density. In the standard DFT calculations, the nonlocal form of the many-electron Fock exchange energy is computed by integrating a local energy density per electron, described by the local electron density and its derivatives.[32,33] One of the most common usages of these generalized gradient approximation (GGA)[34] semi-local functionals is the Perdew-Burke-Ernzerhof (PBE) model,[35] which was later improved by incorporating its exchange energy with a fraction of the exact nonlocal Fock exchange energy,[36] producing hybrid functionals such as PBE0.[37] Among these hybrid functionals, Heyd-Scuseria-Ernzerhof (HSE) screened-Coulomb hybrid density functionals[38–42] take advantage of the short-range HF exchange and avoid computationally expensive long-range exchange. These short-range exchange HSE functionals have shown an appropriate performance to precisely capture the band gap of semiconducting materials.[32,43,44] For this reason, in the current study, we employed both PBE and HSE hybrid functionals to take advantage of computationally efficient and precise DFT techniques to explore the electronic structure of the current CP model.

Recently, the DFT approaches have been broadly utilized to explore the electronic properties of diverse semiconducting polymers.[45,46,55,47–54] Yang and coworkers[56] showed that the DFT

approach can properly estimate the band gap of the CPs having different molecular structures, where the hybrid functional indicated higher accuracy to predict the energy gap. Another DFT study was done on exploring the band gap of several CPs,[52] where the calculated theoretical band gaps show a good agreement with experimental data. In a time-dependent DFT (TD-DFT) study, the simulation successfully predicted the excitation energies and the maximal absorption wavelength of fluorene-based CPs,[57] which were validated by the experimental measurements. DFT and TD-DFT approaches with hybrid functionals were performed to probe the doping process of the polypyrrole,[58] in which the computational results successfully predicted the experimental results on the doping phenomenon. These recent studies have demonstrated that the DFT approach can be utilized as a reliable computational assessment of optoelectronic properties of CPs before experimentally performing a multistep synthesis of these semiconductors. In addition, in the case of polymer materials, the periodicity of the DFT computational model is considerably advantageous for the numerical treatment of polymer structures. For these periodic DFT systems, although sampling of the Brillouin zone via an infinite number of *k*-points is challenging, it can provide suitable convergence to experimental data. An explicit account of the momentum dispersion is a typical technique for 1D periodic models, such as semiconductor nanowires.[59–62]

In the present study, we first explore the ground state properties of the PDPP3T CP using the DFT approach and a one-dimensional single-chain periodic model. Specifically, the PBE and HSE06 hybrid functionals are employed to predict the band gap and absorption spectrum of the system. A basic definition of the conductivity and a classification of the materials such as conductors, insulators, and semiconductors is based on the value of the band gap. A small band gap will allow charge carriers to be promoted from occupied to unoccupied orbitals by thermal excitation or acceleration gained via external voltage AC or DC.[63] We developed our conclusion

based on band gap calculations followed by computing absorption spectrum and charge density distribution. To improve the reliability of our periodic polymer system, the results of band gaps and absorption spectra are numerically treated via momentum sampling over the wide range of k-points in the Brillouin zone.

Additionally, the influences of the charge-carrier injection phenomenon, i.e., mimicking n-type and p-type doping, on the conductivity and absorbance of the polymer model are investigated, which shows that doping plays a critical role in the electrical properties of the semiconductors.[64] We further explore the excitation of the model system by evaluating the electronic properties at the triplet states. Then, the influence of nuclear re-organization induced by the promotion of the electrons from HOMO to LUMO on the energy of the band gap is studied to understand the Stokes shift. The predictive modeling framework established through our study lends valuable insights into the optoelectronic properties of the PDPP3T CPs at both ground and excited states, providing design guidelines for synthesis and processing of novel organic semiconducting materials to achieve tailored performance.

METHODS

Theoretical methods are logically organized into three sections: ground state DFT, computational details, and ground state observables. Some common statements are included in the description for consistency of notations.

Ground state DFT. In the current study, the atomic model is defined by the initial positions of each ion, $\vec{R}_I$. The electronic structure is calculated through the solution of self-consistent equation of density functional theory (DFT)[65] via Vienna Ab initio Simulation Package (VASP).[66] This approach is developed based on a fictitious one-electron Kohn-Sham (KS) equation:

$$\left(-\frac{\hbar^2}{2m}(\nabla-\vec{k})^2+1/[\vec{r}-\vec{R}_I]+v[\vec{r},\,\rho(\vec{r})]\right)\varphi_{i,\vec{k}}^{KS}(\vec{r})=\varepsilon_{i,\vec{k}}\,\varphi_{i,\vec{k}}^{KS}(\vec{r}) \tag{1}$$

where $\rho(\vec{r})$ stands for electronic charge distribution, and $\varphi_{\mathrm{i},\vec{\mathrm{k}}}^{KS}(\vec{\mathrm{r}})$ are electronic states. The solution of the Kohn-Sham equations are single-electron KS orbitals that depend on three spatial variables $\varphi_{i,\vec{k}}^{KS}(\vec{r})$. Then, the solution of Eq. (1) is a set of one-electron momentum dependent orbitals:

$$\varphi_{i,\vec{k}}^{KS}(\vec{r})=e^{i\vec{k}.\vec{r}}\sum_{|\vec{G}|\leq\vec{G}_{cut}}C_{\vec{G},i,\vec{k}}\,e^{i\vec{G}.\vec{r}} \tag{2}$$

where $\vec{G}$ is reciprocal lattice vectors and $\vec{\mathrm{G}}_{\mathrm{cut}}$ stands for a cut-off sphere in reciprocal space. The total density of electrons is calculated from the combination of the orbitals and the orbital occupation function $f_{i,\vec{k}}$.

$$\rho(\vec{r})=\sum_{i,j,\vec{k},\vec{k\prime}}\rho_{i,j,\vec{k},\vec{k\prime}}^{eq}\,\varphi_{i,\vec{k}}^{KS^*}(\vec{r})\varphi_{j,\vec{k}\prime}^{KS}(\vec{r}) \tag{3}$$

$$\rho_{i,j,\vec{k},\vec{k\prime}}^{eq}=\delta_{kk\prime}\delta_{ij}f_{i,\vec{k}} \tag{4}$$

$$f_{i,\vec{k}}=\begin{cases}1 & i\leq HOMO(\vec{k})\\ 0 & i\geq LUMO(\vec{k})\end{cases} \tag{5}$$

where HOMO and LUMO stand for highest occupied molecular orbital and lowest unoccupied molecular orbital, respectively. Then, the total density provides the potential:

$$v[\vec{r},\rho] = {}^{\delta}/_{\delta\rho}\,(E_o^{tot}[\rho] - T[\rho]) \tag{6}$$

The potential is described as a functional derivative of total energy to the variation of total density, which includes interactions of electrons with ions as well as three electron interactions as Coulomb, correlation, and exchange. In the case of hybrid functionals, the HSE functional benefits from the fraction of Fock exchange, a, at zero electron separation and a length scale, $1/\omega$, where the short-range Fock exchange is calculated as follows:

$$E_{XC}^{HSE} = aE_{XC}^{HF,SR}(\omega) + (1-a)E_X^{PBE,SR}(\omega) + E_X^{PBE,LR}(\omega) + E_X^{PBE} \tag{7}$$

The short-range Fock exchange is then computed via the spinful Kohn-Sham density matrix $\rho_{\sigma,\sigma'}(r,r')$:[32]

$$E_{XC}^{HF,SR}(\omega) = -\frac{1}{2}\sum_{\sigma,\sigma'}\int dr dr' \frac{erfc(\omega|r-r'|)}{|r-r'|} \times \left|\rho_{\sigma,\sigma'}(r,r')\right|^2 \tag{8}$$

while the long-range and remaining short-range exchange are determined from the exchange-hole formulation of PBE functionals.[35]

Charge injection. To study the influence of charge-carrier-injection on the optoelectronic properties of the current CP model, we consider two additional configurations with a different number of electrons. The solution of the electronic structure and total energy depends on the number of electrons $N = \int \rho(\vec{r})\, d\vec{r}$. For the neutral CP system utilized in this study, the total number of valence electrons is $N^{\mathrm{Neutral}} = 624$. For the negatively charged system, we consider DFT calculation for a model with two more electrons ($N^{\mathrm{Anion}} = N^{\mathrm{Neutral}} + 2$) by setting the control parameter of "NELECT" to 626 in the VASP software to determine the total number of electrons in the system. In the same manner, for the positively charged system ($N^{\mathrm{Cation}} = N^{\mathrm{Neutral}} - 2$), "NELECT" is set to 622 having a hole-injected DFT model with two fewer

electrons. For each model, the geometry of the system is fully optimized after the charge injection before any characterization. It should be noted that, in the case of manually modified value of the " NELECT " parameter of the charge-injected polymer systems, an additional neutralizing homogeneous background charge is applied by VASP.[67–70]

Triplet state. In the case of triplet (and any non-singlet) electronic configuration, the total number of electrons can be different for spin α and β, where $N_\alpha = \int \rho_\alpha(\vec{r})\, d\vec{r}$ and $N_\beta = \int \rho_\beta(\vec{r})\, d\vec{r}$ are the number of α-electrons and β-electrons, respectively. The sum of $N_\alpha + N_\beta$ should be equal to the total number of electrons, and the difference $\Delta N = N_\alpha - N_\beta$ is often referred to as a spin polarization parameter in the DFT calculations. In the present study, we perform triplet spin state calculations by setting the parameters of " $\mathrm{ISPIN} = 2$ ", and "$NUPDOWN = \Delta N = 2$" in the VASP software. For $\Delta N = 2$, the total spin is $S = \Delta N/2 = 2/2 = 1$, and multiplicity of energy configuration reads $m = 2S + 1 = 2 \times 1 + 1 = 3$ which corresponds to the triplet spin configuration.[71]

Modified occupancy. A promotion of electronic population from HOMO to LUMO, is related to change the population pattern for KS orbitals, maintaining close shell and singlet spin configuration. The vertical excitation is mimicked by such promotion from HOMO to LUMO, where the contribution of each KS orbital to the total density of the system is defined via occupation numbers $\rho(\vec{r}) = \sum_i f_i\, \varphi_i^{KS^*}(\vec{r})\varphi_j^{KS}(\vec{r})$. In general, an excitation from occupied orbital *a* and unoccupied orbital *b* can be described by the diagonal density matrix $\rho_{ij}^{(a,b)} = \delta_{ij}(f_i - \delta_{ia} - \delta_{ib})$ where δ is the Kronecker delta symbol and equilibrium population reads $f_i = \begin{cases} 1 & i \le HOMO \\ 0 & i \ge LUMO \end{cases}$.[72] To perform this, one defines the modified occupancy by setting the "FERWE" parameter in the VASP software, to artificially setup the non-Aufbau occupancies for examining

excited states beyond the lowest-energy occupancy. After resetting the electronic populations, the geometry of the polymer system is optimized before any property calculation.[73–75]

Ground state observables. Momentum dispersion is presented as $\varepsilon_i(\vec{k})$ which is considered in z-direction of polymer model. The partial density of states for a given momentum $\vec{k}$ is computed as follows:

$$D_{\vec{k}}(\varepsilon) = \sum_i \delta\left(\varepsilon - \varepsilon_{i,\vec{k}}\right) \tag{9}$$

where $\varepsilon_{i,\vec{k}}$ represent the energy of a given orbital and the index i runs over all calculated bands. The Dirac delta function $\delta(\varepsilon - \varepsilon_{i,\vec{k}})$ is modeled using a Lorentzian $\delta(x) = \frac{1}{\pi}\frac{\sigma}{\sigma^2+x^2}$.

In the case of spin polarization (SP) DFT calculations, in addition to summations over bands, additional summations over spin up α and spin down β components is taken into account.

$$D_{SP}(\varepsilon) = \sum_{i,\sigma} \delta\left(\varepsilon - \varepsilon_{i,\sigma}^{SP}\right) \tag{10}$$

The Dirac delta function is approximated as a Gaussian distribution to capture the thermal broadening.

The calculation of absorption spectrum is based on the independent orbital approximation IOA in which the optical property of the model is defined by matrix elements of electronic transitions in the basis of auxiliary Kohn-Sham orbitals.[76,77] Lowest energy peak of the computed absorption spectrum is an appropriate quantitative measure of the conductivity since they include the matrix element of the momentum.[78] The absorption spectrum of the polymer model is calculated based

on the consideration of the transitions maintaining momentum conservation $\Delta\vec{k} = 0$ via the following equation:

$$\alpha(\omega) = \sum_{\vec{k}} \alpha_{\vec{k}}(\omega) \tag{11}$$

Equation (11) is formulated in terms of summation of the partial spectra at a given value of momentum $\vec{k}$.

$$\alpha_{\vec{k}}(\omega) = \sum_{ij} f_{ij,\vec{k}}\, \delta(\hbar\omega - |\varepsilon_{i,\vec{k}} - \varepsilon_{j,\vec{k}}|) \tag{12}$$

where $f_{ij,\vec{k}}$ is the probability of electronic transition between states *i* and *j* corresponding to the angular frequency ω of the incident light, referred as oscillator strength between state *i* and *j*;

$$f_{ij,\vec{k}} = \frac{4\pi m_e \omega_{ij,\vec{k}}}{3he^2}\, |\langle \vec{D}_{ij,\vec{k}} \rangle|^2 \tag{13}$$

Here, for a given value of $\vec{k}$ vector, $\langle \vec{D}_{ij,\vec{k}} \rangle$ stands for expectation value of the transition dipole moment.

$$\langle \vec{D}_{ij,k} \rangle = \int \varphi^{KS}_{i,\vec{k}} \vec{r}\, \varphi^{KS}_{j,\vec{k}} d\vec{r} \tag{14}$$

The matrix element of the transition dipole moment correlates the spatial overlap between pair of electronic states *i* and *j* and corresponds to the matrix elements of position operator.[78] The delta function in equation Eq. (12) is approximated as a Lorentzian distribution to account for thermal fluctuations.

Periodic model. The atomistic model of the CP is shown in **Figure 1**. The periodic model consists of the monomers which are connected upon approximately 180° rotation relative to each other, to make adjacent thiophene groups more stable and preserve the linear structure of the backbone

while the same-oriented successive monomers exhibit curvature of the backbone within the conjugated plane.[79] The chemical structure is generated by Materials Studio package pre-optimized via force field calculations. The backbone of the periodic model is stretched in z-direction where the cell-size in that direction is calculated to keep the system at the minimum total energy state. The side groups of C_6H_{13} and C_8H_{17} are grafted to both sides of the monomer. **Figure 1B** shows the geometrically optimized structure of the polymer model.

RESULTS

An illustrative schema of the current study is presented in **Figure 2**. First, as it is shown in **Figure 2a**, the energy gap of the current semiconducting polymer model is explored, and the results are compared to the experimental data. Next, the influence of charge-carrier-injection, mimicking the doping phenomenon, on the fundamental electronic and optical properties of the polymer model is investigated. Doping is the process of adding impurities to the semiconductors to modify their electronic structure. A smaller energy gap between conduction band (CB) and valence band (VB) facilitates moving electrons from HOMO to LUMO under excitation, leading to an increase in the electrical conductivity in semiconductors. Such a phenomenon is directly relevant to the photovoltaic performance of these semiconducting materials. Through the injection of a charge-carrier, a new filled/empty energy level appears between VB and CB, which reduces the band gap and increases the conductivity as shown in **Figure 2b** and **c**. Here, we explore the influence of charge-carrier-injection on the electronic properties of PDPP3T CP to provide useful insights into the optical properties at the excited state, allowing for tunable conductivity of these polymers. Additionally, the triplet state of the polymer model is probed to gain insights into the excitation of these semiconductors (**Figure 2d**). Next, we explore the response of geometry to electronic excitation, i.e., nuclear reorganization, induced by promoting electrons from HOMO to

LUMO, and its influence on the band gap of the polymer model (**Figure 2e**). Finally, for further investigation of the band gap of the ground state and absorption spectrum, momentum sampling (**Figure 2f**) is carried out over the Brillouin zone to properly sample the reciprocal space.

First, to study the ground state band structure and predict the band gap, PBE functional is utilized to minimize the total energy of the system. The density of states (DOS) representing band structure of different electronic configurations of the PDPP3T model are reported in **Figure 3**. The DOS in the energy range near frontier orbitals are exhibited in **Figure 3a**, where a computed band gap of 0.89 eV is found, which is smaller than the experimentally measured band gap of 1.3 eV obtained via the optical absorption.[21] This implies that PBE functional underestimates the value of the bandgap of the current polymer model. Next, the electronic structure is computed via a hybrid HSE06 functional to provide a better prediction of the bandgap compared to the experimental value. The bandgap of 1.2 eV obtained via HSE06 functional, corresponds to DOS shown in **Figure 3b**, agrees reasonably well with the experimental value, highlighting the capabilities of DFT calculations to predict the energy gap of semiconductors. The value of band gap is one of the major factors that determine the electrical conductivity of semiconductors. In the case of low-band gap systems, electrons can be easily promoted from the valence band to the conduction band, and the current can flow.

The results of injection of the negative and positive charge-carriers on the energy gap are reported in **Figure 3c** and **d.** The electronic structure of the injected polymer model is expected to imitate the behavior of doped semiconductors. As **Figure 3c** indicates, after the injection of two electrons into the system, the original LUMO orbital is populated ending in a smaller energy gap of 0.34 eV. This decrease of the band gap indicates that injecting the electrons (n-type doping) can considerably improve the conductivity of the current model, which is consistent with the recent

experimental study of the similar CP system.[80] Negative and positive injections here could correspond to chemical reduction and chemical oxidation in experiments, respectively and also relate to formation of polaron quasiparticle.[81,82]

In a similar manner, we explore the influence of positive charge-carriers injection, mimicking p-type doping, on the energy gap of the current semiconducting CP. **Figure 3d** shows that injecting holes into the system tends to considerably decrease the band gap to 0.29 eV. Indeed, withdrawing two electrons from the system forms a p-type region and evacuates two electrons of HOMO that converts it into a new LUMO* which leads to appearing new energy levels and a smaller band gap. In similar experimental studies on PDPP3T polymer, it was found that p-type doping can significantly improve the conductivity of the system. [83,84]

Then, the triplet state results are presented in **Figure 3e**, where the results for both spin up and down directions point out the band gap of 0.35 eV and 0.29 eV, respectively, implying that the bandgap is decreased in triplet state. To further explore the excited state, the influence of nuclear reorganization on the electronic properties is investigated as shown in **Figure 3f**, where two electrons are promoted from HOMO to LUMO. The optimized geometry under the new condition shows smaller band gaps of 0.49 eV, which corresponds to a higher conductivity for this excited system. Also, the difference in the gaps for the ground and excited configurations $0.89 - 0.49 \approx .4$ eV gives a possible value of Stokes shift for this material.

The DOS plots representing electronic structure of the positively charged, uncharged, and negatively charged polymer model calculated via PBE functional are shown in **Figure 4**. In this figure, all DOS plots are reported for the same energy range to indicate how orbitals are occupied and how energy level is changed after the charge injection. As we go across the progression of the systems with different charges, a larger number of orbitals get occupied. For the positively charged

system, **Figure 4a**, 2 electrons are removed from the system and HOMO label is attributed to the orbital 311. For the uncharged system shown in **Figure 4b**, HOMO label is attributed the orbital 312. Eventually, for the negatively charged system, **Figure 4c**, 2 electrons are injected into the system and occupied the orbital 313 which becomes HOMO. Interestingly, the energy of the orbitals changes as the system gets charged which is interpreted as a signature of the electron-electron interaction. As more orbitals get occupied, Fermi energy shifts up from the lower to higher values. Since principles of the Hohenberg-Kohn theorems of the DFT approach signify and prove the importance of the total energy of the electrons, it would be beneficial to review the total energy of these three systems. For the uncharged system, a total energy of -1519.71 eV is predicted. However, the positively charged system exhibits a total energy of -1510.99 eV, as the model misses electron-electron interactions compared to the uncharged system. The negatively charged system reaches the total energy of -1524.054 eV since the model benefits from two more electrons.

Figure 5 shows the momentum resolved band structure with 16 *k*-points for both PBE and HSE06 functionals. The considered PDPP3T CP model is found to be a direct band gap semiconductor. In the case of PBE functionals, a direct band gap of 0.79 eV is predicted, which underestimates the observed experimental values (as mentioned above). However, for HSE06 functional, a direct gap of 1.2 eV is found to yield a good approximation compared to the experimental values.

Figure 6 exhibits the calculated iso-surfaces of absolute value squared of the four frontier KS orbitals computed via HSE06 functional. A qualitative assessment of the conductivity of a material is affected by two contributions: (a) charge mobility/localization/delocalization and (b) availability of charge carriers in a given band, related to the HOMO/LUMO energy gap. In the current study, both contributions are discussed with more focus on the second contribution. For the orbital

HOMO-1 shown in **Figure 6a**, maximal absolute value squared/charge density appears to be localized on the oxidized dipyrrole group and this localized orbital is not conductive. **Figure 6b** shows HOMO orbital, where the maximum absolute value squared/charge density also resides on the oxidized dipyrrole group. However, there is substantial charge density on each thiophene group, and this delocalized nature of that orbital is expected to contribute to a conductive behavior of the polymer. The LUMO orbital shown in **Figure 6c**, demonstrates maximal value on the oxygen in the pyridine group accompanied by a substantial absolute value squared/charge density on each thiophene and oxidized dipyrrole group. This delocalized nature of this orbital is also expected to contribute to conductive behavior of the polymer.

The absorption spectra of the considered PDPP3T polymer model are reported in **Figure 7**. The fundamental absorption band presented here shows the transition of an electron from the ground state to an excited electronic state. The absorption spectrum describes the probability of an excitation at a certain transition energy. Note that the re-population of orbitals involved in such a transition is used for approximate excited state optimization in what follows. Here, we calculate the oscillator strength and transition energies of the PDPP3T polymer model for both ground and excited states. For the spectrum computed with PBE functional as shown in **Figure 7a**, the first peak appears on 0.8 eV corresponding to the transition energy from HOMO to LUMO. Other peaks of the absorption spectrum correspond to electron promotion pathways between other frontier orbitals. The spectrum computed with HSE06 hybrid functional, **Figure 7b**, shows the first peak equivalent to smallest transition energy of 1.2 eV, which is equal to the calculated band gap between HOMO and LUMO for this functional. The momentum sampling, introduced in **Figure 5**, is computed for both PBE and HSE06 functionals to provide averaged absorption spectra reported in **Figure 7c** and **d**. As **Figure 7c** exhibits, momentum sampling of PBE functional

calculations demonstrates the lowest energy first peak of the absorption spectrum at a transition energy of 0.82 eV. This value corresponds to the predicted direct band gap of 0.79 eV, reported in **Figure 5a,** plus a correction from thermal broadening. On the other hand, **Figure 7d** shows the spectrum computed with momentum sampling using HSE06 functional, and demonstrates the minimum transition energy around 1.32 eV. The absorption spectra of the excited state show the minimum transition energy 0.34 eV and 0.29 eV for models with injected charges, corresponding to n-type and p-type doping, respectively, which is found to be very close to their predicted band gaps in **Figure 3**, see **Figure 7e-f**.

In order to explore the PDPP3T ground state electronic properties, and its optical absorption as well as to compare our results to the available experimental findings, we evaluate the absorption spectra in terms of wavelength, see **Figure 8**. The fundamental absorption wavelength of a semiconductor corresponds to the bandgap value and usually appears in the visible and near IR spectral range. **Figure 8a** shows the absorption spectrum computed with PBE functional, in which maximum absorbance (λ_p) appears around 1400 nm, away from the reported experimental value of $\lambda_p \approx 800$ nm.[85] Furthermore, the absorption spectra computed using HSE06 functional as shown in **Figure 8B**, provides an improved value of $\lambda_p = 1036$ nm compared to the value from PBE functional; however, it still represents a considerable deviation from the experimental data. To improve these results, we calculate the averaged absorption spectrum averaged via momentum sampling, resulting in a better approximation of λ_p, which alleviates the challenge of discrepancy between the computational results and experimental data. In the case of spectrum obtained via sampling and PBE functional, **Figure 8c**, we do not observe any improvement, comparing to the results at the gamma point. However, the spectrum computed with k-point sampling and HSE06

functional provides an improved value of $\lambda_p \approx 737$ nm, which is found to be in good agreement with the experimental data, marked by the black dashed line in **Figure 8d**.

Moreover, **Figure 8e** and **f** show a large red-shift of the absorption spectra wavelength in presence of the injected charges, analogous to n-type and p-type doping of the polymer model. The results imply that the wavelengths of doped PDPP3T absorption spectra will no longer remain in the visible/near IR spectral range and shift into the IR region. A similar trend for this polymer system was observed in experimental studies,[83,84] where the doped PDPP3T polymer exhibited a strong absorption in the IR spectral range.

DISCUSSION

The dependence of electronic properties on the size of the model is important for finite length oligomers and taken into account in periodic models. For finite oligomers, at a certain system size, the bandgap experiences saturation and becomes independent of further increase of the size of the model. In the case of a periodic model, the motion of electrons is restricted in the direction normal/orthogonal to the growth directions and the carriers (electrons) are free to move only in the growth directions (in direction of polymer backbone).

Trends in band gap as function of method. Typically, GGA based PBE exchange-correlation functional underestimates the band gap. The underestimated band gap can be improved by calculating electronic structure using a hybrid functional. In our study, band structure calculation with PBE functional underestimates the band gap of PDPP3T polymer by around 0.41 eV. However, HSE06 functional predicts the bandgap value of 1.2 eV, reasonably close to the experimentally measured value of 1.3 eV.

Trends in band gap as function of physical conditions. Injection of additional electrons and holes (mimicking n-type and p-type doping) is responsible for decreasing the bandgap value. This further implies that the increase of the concentration of injected charge carriers or dopants improves charge carrier mobility in the injected PDPP3T resulting in higher conductivities, which have been experimentally explored before. Generally, charge injection corresponds to oxidation or reduction of the polymer, which means electrons are added to the π^* band or removed from the π band, in an analogy with doping phenomenon; nevertheless, here, the polymer is not directly doped in the sense of chemical or electrochemical doping.[25,26] Besides, the injected PDPP3T polymer with a lower band gap exhibits a shift of absorption spectrum into the IR spectral range, corresponding to a change of semiconductor's color upon the doping. This potentially makes them appropriate material candidates for the development of transparent electronic devices. The absorption spectrum calculated with momentum sampling under HSE06 hybrid functional, demonstrates computed value of λ_p close to the reported experimental values. Additionally, the band gap of the polymer model becomes smaller via two additional mechanisms: nuclear reorganization induced by promoting the electrons from HOMO to LUMO and by formation of triplet state.

Our results provide computational design guidance for development of high-performance D-A semiconducting polymers. Band gap results obtained with HSE06 functional and sampling of the Brillouin zone indicate ~~the~~ capability of the current approach to predict the band gap and absorption spectra of conjugated polymers. The charge injection modeling which is mimicking the doping process is found to be a key driving factor for obtaining low band gap and high-mobility of PDPP3T polymers.

CONCLUSIONS

In the present study, the fundamental electronic and optical properties of the PDPP3T CP are studied via the DFT-based computational approach. The energy gap and absorption spectrum of the ground and excited states are carried out by the PBE and HSE06 hybrid functionals. HSE06 functional yields a noticeable improved prediction of a band gap of 1.2 eV, which is consistent with the experimental value of 1.3 eV for the PDPP3T polymer. The explicit treatment of momentum dispersion under HSE06 functional provides an appropriate agreement of the computed absorption spectrum with the experimental data. Additionally, the paper discusses the analogy between charge injection and of n-type and p-type doping on the optoelectronic properties of the semiconducting polymer model. This analogy is supported by computed evidence that injection of holes and electrons into the polymer can both effectively reduce the band gap and shift absorption spectrum into the IR region. Such change of the electronic structure correlates to increases in conductivity in agreement with experimental observations. This observation is further confirmed by evaluations of nuclear reorganization and triplet state. The reported results demonstrate the efficacy of introducing charge carriers into the PDPP3T as a computationally-guided design strategy to tune the optical and electronic properties and achieve a lower band gap, which are useful in development of high-performance organic photovoltaic and optoelectronic devices.

ACKNOWLEDGMENTS

A.A., F.F., W.X. acknowledge support from the North Dakota Established Program to Stimulate Competitive Research (ND EPSCoR) through the New Faculty Award, the Department of Civil & Environmental Engineering, and the College of Engineering at North Dakota State University (NDSU). The supercomputing resources of the National Energy Research Scientific Computing Center (NERSC), a U.S. Department of Energy Office of Science User Facility located at Lawrence Berkeley National Laboratory DE-AC02-05CH11231 via allocation award "*Computational Modeling of Photo-catalysis and Photo-induced Charge Transfer Dynamics on Surfaces*" and CCAST Thunder Cluster at NDSU are acknowledged. Authors thank Yulun Han, Aaron Forde, and Meade Ericksen for discussions and editorial comments. D.K. thanks Svetlana Kilina, David Micha, Sergei Tretiak, Oleg Prezhdo, Andriy Zhugayevych for inspiring discussions. D.K. acknowledges support of NSF CHE-1944921 and DOE DE-SC0021287. Editorial help of Boston Heaford is gratefully acknowledged.

REFERENCES

(1) Mei, J.; Diao, Y.; Appleton, A. L.; Fang, L.; Bao, Z. Integrated Materials Design of Organic Semiconductors for Field-Effect Transistors. *J. Am. Chem. Soc.* **2013**, *135* (18), 6724–6746. https://doi.org/10.1021/ja400881n.

(2) Sirringhaus, H. 25th Anniversary Article: Organic Field-Effect Transistors: The Path beyond Amorphous Silicon. *Adv. Mater.* **2014**, *26* (9), 1319–1335. https://doi.org/10.1002/adma.201304346.

(3) Xue, X.; Chandler, G.; Zhang, X.; Kline, R. J.; Fei, Z.; Heeney, M.; Diemer, P. J.; Jurchescu, O. D.; O'connor, B. T. Oriented Liquid Crystalline Polymer Semiconductor Films with Large Ordered Domains. *ACS Appl. Mater. Interfaces* **2015**, *7* (48), 26726–26734. https://doi.org/10.1021/acsami.5b08710.

(4) Gu, X.; Shaw, L.; Gu, K.; Toney, M. F.; Bao, Z. The Meniscus-Guided Deposition of Semiconducting Polymers. *Nat. Commun.* **2018**, *9* (1), 534. https://doi.org/10.1038/s41467-018-02833-9.

(5) Sirringhaus, H.; Tessler, N.; Friend, R. H. Integrated Optoelectronic Devices Based on Conjugated Polymers. *Science (80-.).* **1998**, *280* (5370), 1741–1744.

(6) Yamashita, Y.; Hinkel, F.; Marszalek, T.; Zajaczkowski, W.; Pisula, W.; Baumgarten, M.; Matsui, H.; Müllen, K.; Takeya, J. Mobility Exceeding 10 Cm2/(V·s) in Donor-Acceptor Polymer Transistors with Band-like Charge Transport. *Chem. Mater.* **2016**, *28* (2), 420–424. https://doi.org/10.1021/acs.chemmater.5b04567.

(7) Kim, G.; Kang, S. J.; Dutta, G. K.; Han, Y. K.; Shin, T. J.; Noh, Y. Y.; Yang, C. A

Thienoisoindigo-Naphthalene Polymer with Ultrahigh Mobility of 14.4 Cm 2 /V·s That Substantially Exceeds Benchmark Values for Amorphous Silicon Semiconductors. *J. Am. Chem. Soc.* **2014**, *136* (26), 9477–9483. https://doi.org/10.1021/ja504537v.

(8) Luo, C.; Kyaw, A. K. K.; Perez, L. A.; Patel, S.; Wang, M.; Grimm, B.; Bazan, G. C.; Kramer, E. J.; Heeger, A. J. General Strategy for Self-Assembly of Highly Oriented Nanocrystalline Semiconducting Polymers with High Mobility. *Nano Lett.* **2014**, *14* (5), 2764–2771. https://doi.org/10.1021/nl500758w.

(9) Meng, L.; Zhang, Y.; Wan, X.; Li, C.; Zhang, X.; Wang, Y.; Ke, X.; Xiao, Z.; Ding, L.; Xia, R.; Yip, H. L.; Cao, Y.; Chen, Y. Organic and Solution-Processed Tandem Solar Cells with 17.3% Efficiency. *Science (80-.).* **2018**, *361* (6407), 1094–1098. https://doi.org/10.1126/science.aat2612.

(10) Zhugayevych, A.; Tretiak, S. Theoretical Description of Structural and Electronic Properties of Organic Photovoltaic Materials. *Annu. Rev. Phys. Chem.* **2015**, *66* (December), 305–330. https://doi.org/10.1146/annurev-physchem-040214-121440.

(11) Root, S. E.; Savagatrup, S.; Printz, A. D.; Rodriquez, D.; Lipomi, D. J. Mechanical Properties of Organic Semiconductors for Stretchable, Highly Flexible, and Mechanically Robust Electronics. *Chem. Rev.* **2017**, *117* (9), 6467–6499. https://doi.org/10.1021/acs.chemrev.7b00003.

(12) Someya, T.; Bao, Z.; Malliaras, G. G. The Rise of Plastic Bioelectronics. *Nature* **2016**, *540* (7633), 379–385. https://doi.org/10.1038/nature21004.

(13) Lipomi, D. J.; Bao, Z. Stretchable and Ultraflexible Organic Electronics. *MRS Bull.* **2017**, *42* (2), 93–97. https://doi.org/10.1557/mrs.2016.325.

(14) Bao, Z.; Chen, X. Flexible and Stretchable Devices. *Adv. Mater.* **2016**, *28* (22), 4177–4179. https://doi.org/10.1002/adma.201601422.

(15) Oh, J. Y.; Bao, Z. Second Skin Enabled by Advanced Electronics. *Adv. Sci.* **2019**, *6* (11), 1900186. https://doi.org/10.1002/advs.201900186.

(16) Lipomi, D. J.; Tee, B. C. K.; Vosgueritchian, M.; Bao, Z. Stretchable Organic Solar Cells. *Adv. Mater.* **2011**, *23* (15), 1771–1775. https://doi.org/10.1002/adma.201004426.

(17) Chortos, A.; Liu, J.; Bao, Z. Pursuing Prosthetic Electronic Skin. *Nat. Mater.* **2016**, *15* (9), 937–950. https://doi.org/10.1038/nmat4671.

(18) Zhang, S.; Alesadi, A.; Selivanova, M.; Cao, Z.; Qian, Z.; Luo, S.; Galuska, L.; Teh, C.; Ocheje, M. U.; Mason, G. T.; St. Onge, P. B. J.; Zhou, D.; Rondeau-Gagné, S.; Xia, W.; Gu, X. Toward the Prediction and Control of Glass Transition Temperature for Donor–Acceptor Polymers. *Adv. Funct. Mater.* **2020**, *2002221*, 2002221. https://doi.org/10.1002/adfm.202002221.

(19) Zhang, S.; Alesadi, A.; Mason, G. T.; Chen, K.-L.; Freychet, G.; Galuska, L.; Cheng, Y.-H.; St. Onge, P. B. J.; Ocheje, M. U.; Ma, G.; Qian, Z.; Dhakal, S.; Ahmad, Z.; Wang, C.; Chiu, Y.-C.; Rondeau-Gagné, S.; Xia, W.; Gu, X. Molecular Origin of Strain-Induced Chain Alignment in PDPP-Based Semiconducting Polymeric Thin Films. *Adv. Funct. Mater. n/a* (n/a), 2100161. https://doi.org/https://doi.org/10.1002/adfm.202100161.

(20) Chen, H.; Guo, Y.; Yu, G.; Zhao, Y.; Zhang, J.; Gao, D.; Liu, H.; Liu, Y. Highly π-Extended Copolymers with Diketopyrrolopyrrole Moieties for High-Performance Field-Effect Transistors. *Adv. Mater.* **2012**, *24* (34), 4618–4622. https://doi.org/10.1002/adma.201201318.

(21) Bijleveld, J. C.; Zoombelt, A. P.; Mathijssen, S. G. J.; Wienk, M. M.; Turbiez, M.; de Leeuw, D. M.; Janssen, R. A. J. Poly (Diketopyrrolopyrrole− Terthiophene) for Ambipolar Logic and Photovoltaics. *J. Am. Chem. Soc.* **2009**, *131* (46), 16616–16617.

(22) Yim, K.; Whiting, G. L.; Murphy, C. E.; Halls, J. J. M.; Burroughes, J. H.; Friend, R. H.; Kim, J. Controlling Electrical Properties of Conjugated Polymers via a Solution-Based P-Type Doping. *Adv. Mater.* **2008**, *20* (17), 3319–3324.

(23) Salzmann, I.; Heimel, G.; Oehzelt, M.; Winkler, S.; Koch, N. Molecular Electrical Doping of Organic Semiconductors: Fundamental Mechanisms and Emerging Dopant Design Rules. *Acc. Chem. Res.* **2016**, *49* (3), 370–378.

(24) Jayasundara, W. S. R.; Schreckenbach, G. Theoretical Study of P-and n-Doping of Polythiophene-and Polypyrrole-Based Conjugated Polymers. *J. Phys. Chem. C* **2020**, *124* (32), 17528–17537.

(25) Heeger, A. J. Semiconducting and Metallic Polymers: The Fourth Generation of Polymeric Materials. *Curr. Appl. Phys.* **2001**, *1* (4–5), 247–267. https://doi.org/10.1016/S1567-1739(01)00053-0.

(26) Heeger, A. J.; MacDiarmid, A. G.; Shirakawa, H. The Nobel Prize in Chemistry, 2000: Conductive Polymers. *Stock. Sweden R. Swedish Acad. Sci.* **2000**, 1–16.

(27) Kim, B.; Ma, X.; Chen, C.; Ie, Y.; Coir, E. W.; Hashemi, H.; Aso, Y.; Green, P. F.; Kieffer, J.; Kim, J. Energy Level Modulation of HOMO, LUMO, and Band-gap in Conjugated Polymers for Organic Photovoltaic Applications. *Adv. Funct. Mater.* **2013**, *23* (4), 439–445.

(28) Ma, X.; Lv, Y.; Xu, J.; Liu, Y.; Zhang, R.; Zhu, Y. A Strategy of Enhancing the Photoactivity of G-C3N4 via Doping of Nonmetal Elements: A First-Principles Study. *J. Phys. Chem. C* **2012**, *116* (44), 23485–23493.

(29) Medvedev, M. G.; Bushmarinov, I. S.; Sun, J.; Perdew, J. P.; Lyssenko, K. A. Density Functional Theory Is Straying from the Path toward the Exact Functional. *Science (80-.).* **2017**, *355* (6320), 49–52.

(30) Jones, R. O. Density Functional Theory: Its Origins, Rise to Prominence, and Future. *Rev. Mod. Phys.* **2015**, *87* (3), 897.

(31) Hohenberg, P. P Hys. Rev. 1964, 136, B864–B871; b) w. Kohn, Lj Sham. *Phys. Rev* **1965**, *140*, A1133–A1138.

(32) Moussa, J. E.; Schultz, P. A.; Chelikowsky, J. R. Analysis of the Heyd-Scuseria-Ernzerhof Density Functional Parameter Space. *J. Chem. Phys.* **2012**, *136* (20), 204117.

(33) Sholl, D.; Steckel, J. A. *Density Functional Theory: A Practical Introduction*; John Wiley & Sons, 2011.

(34) Perdew, J. P. Accurate Density Functional for the Energy: Real-Space Cutoff of the Gradient Expansion for the Exchange Hole. *Phys. Rev. Lett.* **1985**, *55* (16), 1665.

(35) Perdew, J. P.; Burke, K.; Ernzerhof, M. Generalized Gradient Approximation Made Simple. *Phys. Rev. Lett.* **1996**, *77* (18), 3865.

(36) Becke, A. D. Becke's Three Parameter Hybrid Method Using the LYP Correlation Functional. *J. Chem. Phys* **1993**, *98* (492), 5648–5652.

(37) Adamo, C.; Barone, V. Toward Reliable Density Functional Methods without Adjustable

Parameters: The PBE0 Model. *J. Chem. Phys.* **1999**, *110* (13), 6158–6170.

(38) Heyd, J.; Scuseria, G. E.; Ernzerhof, M. No Title. *J. Chem. Phys.* **2003**, *118*, 8207.

(39) Heyd, J.; Scuseria, G. E.; Ernzerhof, M. No Title. *J. Chem. Phys.* **2006**, *124*, 219906.

(40) Heyd, J.; Scuseria, G. E. No Title. *J. Chem. Phys.* **2004**, *120*, 7274.

(41) Heyd, J.; Scuseria, G. E. No Title. *J. Chem. Phys.* **2004**, *121*, 1187.

(42) Heyd, J.; Peralta, J. E.; Scuseria, G. E.; Martin, R. L. No Title. *J. Chem. Phys.* **2005**, *123*, 174101.

(43) Heyd, J.; Peralta, J. E.; Scuseria, G. E.; Martin, R. L. Energy Band Gaps and Lattice Parameters Evaluated with the Heyd-Scuseria-Ernzerhof Screened Hybrid Functional. *J. Chem. Phys.* **2005**, *123* (17), 174101. https://doi.org/10.1063/1.2085170.

(44) Paier, J.; Marsman, M.; Hummer, K.; Kresse, G.; Gerber, I. C.; Ángyán, J. G. Screened Hybrid Density Functionals Applied to Solids. *J. Chem. Phys.* **2006**, *124* (15), 154709.

(45) Siham, L.; Bouchra, M.; Latfa, L.; Ahmed, J. Electronic and Photoelectronic Properties of N-(5-Indazolyl)-Arylsulfonamides Molecules: DFT/TD-DFT Study. In *2020 IEEE 6th International Conference on Optimization and Applications (ICOA)*; IEEE, 2020; pp 1–6.

(46) Vu, Q.-T.; Tran, T.-T.-D.; Nguyen, T.-C.; Nguyen, T. V.; Nguyen, H.; Vinh, P. Van; Nguyen-Trong, D.; Dinh Duc, N.; Nguyen-Tri, P. DFT Prediction of Factors Affecting the Structural Characteristics, the Transition Temperature and the Electronic Density of Some New Conjugated Polymers. *Polymers (Basel).* **2020**, *12* (6), 1207.

(47) Vu, K. B.; Vu, V. V; Thu, H. P. T.; Giang, H. N.; Tam, N. M.; Ngo, S. T. Conjugated Polymers: A Systematic Investigation of Their Electronic and Geometric Properties Using

Density Functional Theory and Semi-Empirical Methods. *Synth. Met.* **2018**, *246*, 128–136.

(48) Sun, H.; Autschbach, J. Electronic Energy Gaps for π-Conjugated Oligomers and Polymers Calculated with Density Functional Theory. *J. Chem. Theory Comput.* **2014**, *10* (3), 1035–1047. https://doi.org/10.1021/ct4009975.

(49) Mabrouk, A.; Azazi, A.; Alimi, K. Molecular Structure–Property Engineering of Low-band-gap Copolymers, Based on Fluorene, for Efficient Bulk Heterojunction Solar Cells: A Density Functional Theory Study. *Polym. Eng. Sci.* **2013**, *53* (5), 1040–1052.

(50) Ferretti, A.; Mallia, G.; Martin-Samos, L.; Bussi, G.; Ruini, A.; Montanari, B.; Harrison, N. M. Ab Initio Complex Band Structure of Conjugated Polymers: Effects of Hydrid Density Functional Theory and GW Schemes. *Phys. Rev. B* **2012**, *85* (23), 235105.

(51) Risko, C.; McGehee, M. D.; Brédas, J.-L. A Quantum-Chemical Perspective into Low Optical-Gap Polymers for Highly-Efficient Organic Solar Cells. *Chem. Sci.* **2011**, *2* (7), 1200–1218.

(52) Zhang, L.; Zhang, Q.; Ren, H.; Yan, H.; Zhang, J.; Zhang, H.; Gu, J. Calculation of Band Gap in Long Alkyl-Substituted Heterocyclic-Thiophene-Conjugated Polymers with Electron Donor–Acceptor Fragment. *Sol. energy Mater. Sol. cells* **2008**, *92* (5), 581–587.

(53) Darling, S. B. Isolating the Effect of Torsional Defects on Mobility and Band Gap in Conjugated Polymers. *J. Phys. Chem. B* **2008**, *112* (30), 8891–8895.

(54) Gierschner, J.; Cornil, J.; Egelhaaf, H. Optical Bandgaps of Π-conjugated Organic Materials at the Polymer Limit: Experiment and Theory. *Adv. Mater.* **2007**, *19* (2), 173–191.

(55) Kilina, S.; Kilin, D.; Tretiak, S. Light-Driven and Phonon-Assisted Dynamics in Organic and Semiconductor Nanostructures. *Chem. Rev.* **2015**, *115* (12), 5929–5978. https://doi.org/10.1021/acs.chemrev.5b00012.

(56) Yang, S.; Olishevski, P.; Kertesz, M. Bandgap Calculations for Conjugated Polymers. *Synth. Met.* **2004**, *141* (1–2), 171–177.

(57) Wang, J.-F.; Feng, J.-K.; Ren, A.-M.; Liu, X.-D.; Ma, Y.-G.; Lu, P.; Zhang, H.-X. Theoretical Studies of the Absorption and Emission Properties of the Fluorene-Based Conjugated Polymers. *Macromolecules* **2004**, *37* (9), 3451–3458.

(58) Ullah, H.; Shah, A.-H. A.; Bilal, S.; Ayub, K. Doping and Dedoping Processes of Polypyrrole: DFT Study with Hybrid Functionals. *J. Phys. Chem. C* **2014**, *118* (31), 17819–17830.

(59) Fatima; Vogel, D. J.; Han, Y.; Inerbaev, T. M.; Oncel, N.; Kilin, D. S. First-Principles Study of Electron Dynamics with Explicit Treatment of Momentum Dispersion on Si Nanowires along Different Directions. *Mol. Phys.* **2019**, *117* (17), 2293–2302.

(60) Fatima; Vogel, J.; Inerbaev, T.; Oncel, N.; Kilin, D. First-Principles Study of Charge Carrier Dynamics with Explicit Treatment of Momentum Dispersion on Si Nanowires Along< 211> Crystallographic Directions. *MRS Adv.* **2018**, *3* (59), 3477–3482.

(61) Fatima; Forde, A.; Inerbaev, T. M.; Oncel, N.; Kilin, D. S. Time-Resolved Optical Properties of SiNW Oriented In< 211> Crystallographic Direction. *MRS Adv.* **2019**, *4* (36), 2009–2014.

(62) Fatima; Han, Y.; Vogel, D. J.; Inerbaev, T. M.; Oncel, N.; Hobbie, E. K.; Kilin, D. S.

Photoexcited Electron Lifetimes Influenced by Momentum Dispersion in Silicon Nanowires. *J. Phys. Chem. C* **2019**, *123* (12), 7457–7466.

(63) Cardona, M.; Peter, Y. Y. *Fundamentals of Semiconductors*; Springer, 2005.

(64) Kar, P. *Doping in Conjugated Polymers*; John Wiley & Sons, 2013.

(65) Hohenberg, P.; Kohn, W. Inhomogeneous Electron Gas Physical Review 136. *B864* **1964**.

(66) Kresse, G.; Furthmüller, J. Efficient Iterative Schemes for Ab Initio Total-Energy Calculations Using a Plane-Wave Basis Set. *Phys. Rev. B* **1996**, *54* (16), 11169.

(67) Meng, Q.; Chen, J.; Kilin, D. Proton Reduction at Surface of Transition Metal Nanocatalysts. *Mol. Simul.* **2015**, *41* (1–3), 134–145.

(68) Makov, G.; Payne, M. C. Periodic Boundary Conditions in Ab Initio Calculations. *Phys. Rev. B* **1995**, *51* (7), 4014.

(69) Neugebauer, J.; Scheffler, M. Adsorbate-Substrate and Adsorbate-Adsorbate Interactions of Na and K Adlayers on Al (111). *Phys. Rev. B* **1992**, *46* (24), 16067.

(70) Brown, S. L.; Hobbie, E. K.; Tretiak, S.; Kilin, D. S. First-Principles Study of Fluorescence in Silver Nanoclusters. *J. Phys. Chem. C* **2017**, *121* (43), 23875–23885.

(71) Yao, G.; Berry, M. T.; May, P. S.; Kilin, D. DFT Calculation of Russell–Saunders Splitting for Lanthanide Ions Doped in Hexagonal (β)-NaYF4 Nanocrystals. *J. Phys. Chem. C* **2013**, *117* (33), 17177–17185.

(72) Jensen, S. J.; Inerbaev, T. M.; Kilin, D. S. Spin Unrestricted Excited State Relaxation Study of Vanadium (IV)-Doped Anatase. *J. Phys. Chem. C* **2016**, *120* (11), 5890–5905.

(73) Chen, J.; Meng, Q.; Stanley May, P.; Berry, M. T.; Kilin, D. S. Time-Dependent Excited-State Molecular Dynamics of Photodissociation of Lanthanide Complexes for Laser-Assisted Metal-Organic Chemical Vapour Deposition. *Mol. Phys.* **2014**, *112* (3–4), 508–517.

(74) Han, Y.; Anderson, K.; Hobbie, E. K.; Boudjouk, P.; Kilin, D. S. Unraveling Photodimerization of Cyclohexasilane from Molecular Dynamics Studies. *J. Phys. Chem. Lett.* **2018**, *9* (15), 4349–4354.

(75) Han, Y.; Rasulev, B.; Kilin, D. S. Photofragmentation of Tetranitromethane: Spin-Unrestricted Time-Dependent Excited-State Molecular Dynamics. *J. Phys. Chem. Lett.* **2017**, *8* (14), 3185–3192.

(76) Vogel, D. J.; Kryjevski, A.; Inerbaev, T.; Kilin, D. S. Photoinduced Single-and Multiple-Electron Dynamics Processes Enhanced by Quantum Confinement in Lead Halide Perovskite Quantum Dots. *J. Phys. Chem. Lett.* **2017**, *8* (13), 3032–3039.

(77) Han, Y.; Meng, Q.; Rasulev, B.; May, P. S.; Berry, M. T.; Kilin, D. S.; Vogel, D. J.; Kryjevski, A.; Inerbaev, T.; Kilin, D. S.; Han, Y.; Meng, Q.; Rasulev, B.; May, P. S.; Berry, M. T.; Kilin, D. S. Photoinduced Charge Transfer versus Fragmentation Pathways in Lanthanum Cyclopentadienyl Complexes. *J. Chem. Theory Comput.* **2017**, *8* (13), 4281–4296.

(78) Kilin, D. S.; Tsemekhman, K. L.; Kilina, S. V; Balatsky, A. V; Prezhdo, O. V. Photoinduced Conductivity of a Porphyrin− Gold Composite Nanowire. *J. Phys. Chem. A* **2009**, *113* (16), 4549–4556.

(79) Vezie, M. S.; Few, S.; Meager, I.; Pieridou, G.; Dörling, B.; Ashraf, R. S.; Goñi, A. R.;

Bronstein, H.; McCulloch, I.; Hayes, S. C.; Campoy-Quiles, M.; Nelson, J. Exploring the Origin of High Optical Absorption in Conjugated Polymers. *Nat. Mater.* **2016**, *15* (7), 746–753. https://doi.org/10.1038/nmat4645.

(80) Huseynova, G.; Shin, E. Y.; Park, W. T.; Noh, Y. Y. Lithium Benzoate Doped High Performance N-Type Diketopyrrolopyrrole Based Organic Thin-Film Transistors. *Dye. Pigment.* **2019**, *162* (October 2018), 243–248. https://doi.org/10.1016/j.dyepig.2018.10.032.

(81) Forde, A.; Inerbaev, T.; Kilin, D. Spectral Signatures of Positive and Negative Polarons in Lead-Halide Perovskite Nanocrystals. *J. Phys. Chem. C* **2019**, *124* (1), 1027–1041.

(82) Guo, J.; Ohkita, H.; Benten, H.; Ito, S. Near-IR Femtosecond Transient Absorption Spectroscopy of Ultrafast Polaron and Triplet Exciton Formation in Polythiophene Films with Different Regioregularities. *J. Am. Chem. Soc.* **2009**, *131* (46), 16869–16880.

(83) Karpov, Y.; Erdmann, T.; Raguzin, I.; Al-Hussein, M.; Binner, M.; Lappan, U.; Stamm, M.; Gerasimov, K. L.; Beryozkina, T.; Bakulev, V. High Conductivity in Molecularly P-Doped Diketopyrrolopyrrole-Based Polymer: The Impact of a High Dopant Strength and Good Structural Order. *Adv. Mater.* **2016**, *28* (28), 6003–6010.

(84) Jung, I. H.; Hong, C. T.; Lee, U.-H.; Kang, Y. H.; Jang, K.-S.; Cho, S. Y. High Thermoelectric Power Factor of a Diketopyrrolopyrrole-Based Low Bandgap Polymer via Finely Tuned Doping Engineering. *Sci. Rep.* **2017**, *7*, 44704.

(85) Hofmann, A. I.; Kroon, R.; Zokaei, S.; Järsvall, E.; Malacrida, C.; Ludwigs, S.; Biskup, T.; Müller, C. Chemical Doping of Conjugated Polymers with the Strong Oxidant Magic Blue. *Adv. Electron. Mater.* **2020**, *6* (8), 1–8. https://doi.org/10.1002/aelm.202000249.

FIGURES AND TABLES

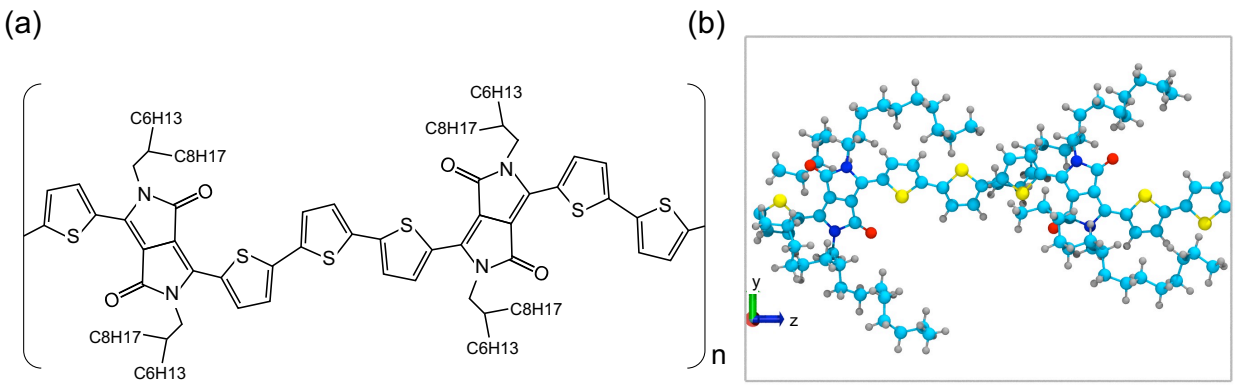

Figure 1. (a) Schematic chemical structure of the PDPP conjugated polymer model employed in the simulations. **(b)** Geometry optimized structure (ground state) of the polymer model aligned in the y-z plane. Cyan, blue, gray, yellow, and red spheres represent C, N, H, S, and O atoms respectively.

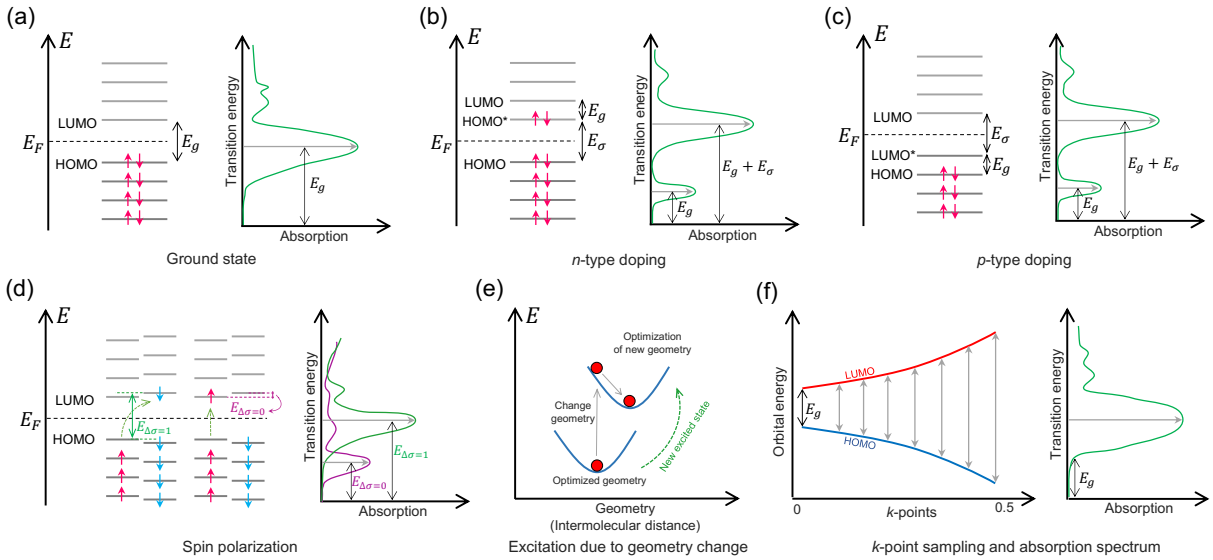

Figure 2. (a) A schematic of the ground state energy band and absorption spectra. **(b)** The schema of the energy band and absorption spectra due to n-type doping (electron donors). **(c)** The schema of the energy band and absorption spectra due to p-type doping (electron acceptors). **(d)** Schema of spin polarization process and corresponding absorption spectra. **(e)** A portrayal of change of geometry due to excitation and optimized geometry after the excitation. **(f)** A schematic representation of band structure with *k*-points sampling and corresponding absorption spectrum. Here, E_g, E_F, E_σ, and $E_{\Delta\sigma}$ represents band gap energy, Fermi energy, and band energy gap of excited state, respectively.

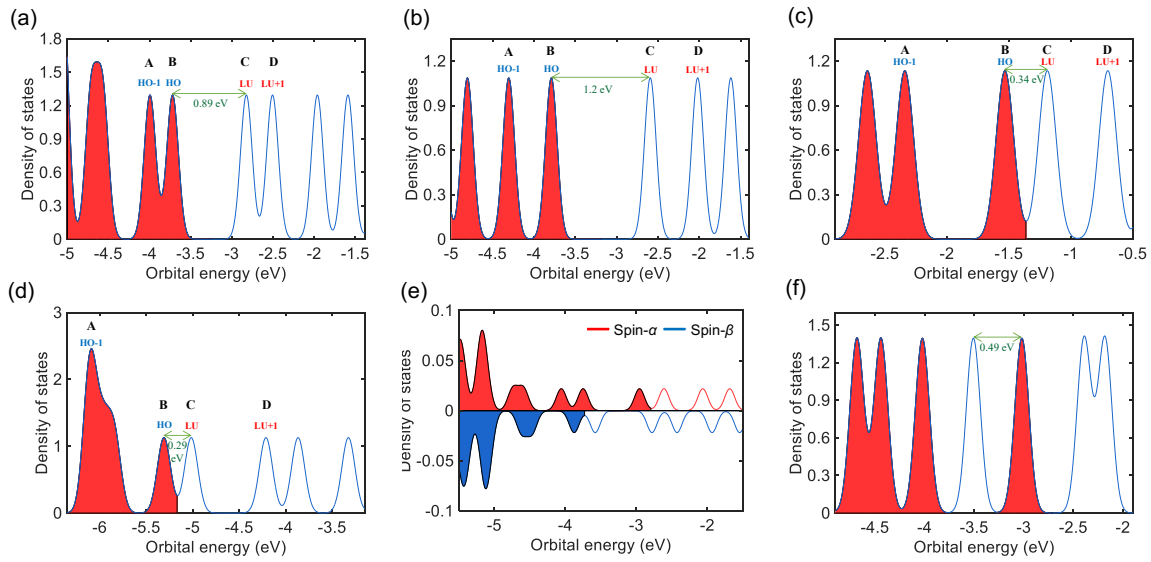

Figure 3. (a) DOS of the polymer model calculated by DFT via PBE exchange-correlation functional. Red shaded regions represent the occupied orbitals and unshaded regions indicate unoccupied orbitals. Four frontier orbitals near the band gap are labeled. **(b)** DOS of polymer model calculated by DFT via HSE06 hybrid functional in which band gap is larger. **(c)** DOS of polymer model calculated by DFT for the injected electron doping of the conjugated polymer model (n-doping, negative polaron). Red shaded regions represent the occupied orbitals and unshaded regions indicate unoccupied orbitals. Four frontier orbitals near the band gap are labeled. **(d)** DOS of polymer model calculated by DFT for the injected hole doping (p-doping, positive polaron) of the conjugated polymer model. **(e)** Triplet state DOS of the CP model. The red-shaded regions indicate the occupied orbitals with spin +1/2 and blue shaded regions correspond to spin

component -1/2. **(f)** DOS near the band edges of the CP model when an electron was promoted from HOMO to LUMO, mimicking excited state.

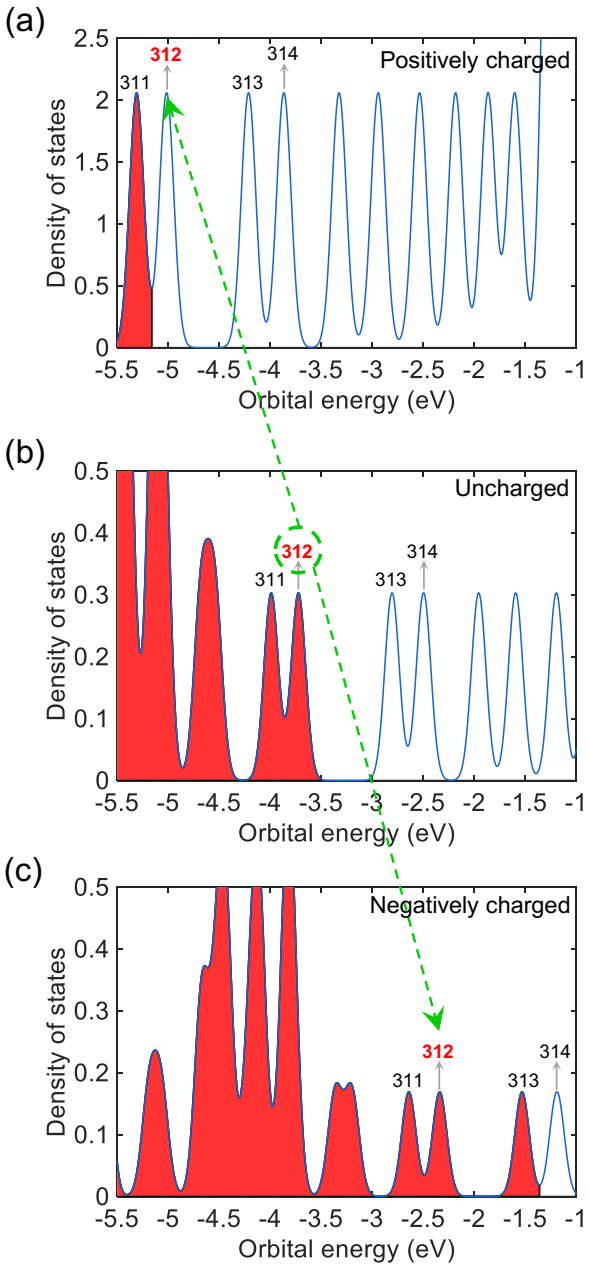

Figure 4. DOS of the **(a)** positively charged **(b)** uncharged and **(c)** negatively charged polymer models calculated via PBE functional. All three DOS are plotted for the same energy level to show

how near-gap orbitals are populated and how the energy level is shifted upon the charge injection. Red shaded regions represent the occupied orbitals. The orbital number of four frontier orbitals near the band gap is shown.

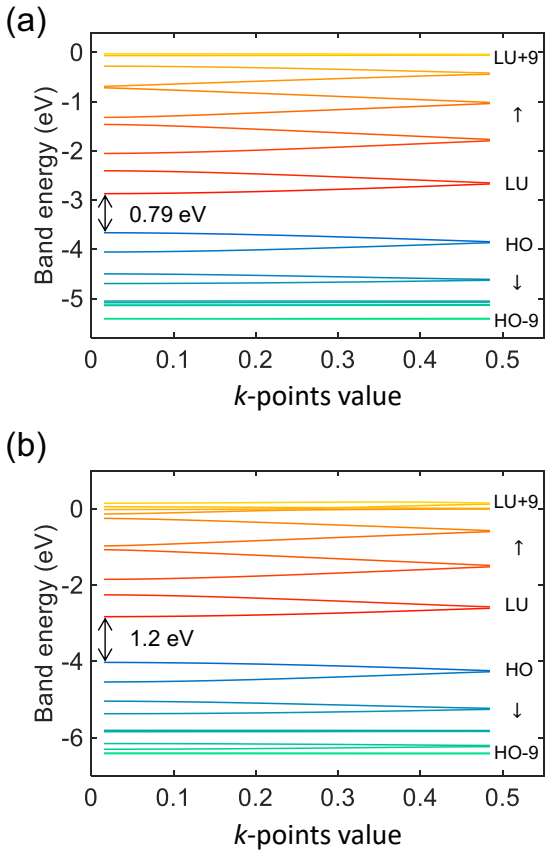

Figure 5. (a) The band structure of a reference CP model calculated using PBE functional. A direct band gap is predicted. **(b)** The band structure of the same model was calculated through HSE06 functional. In both cases, the x-axis represents *k*-point sampling.

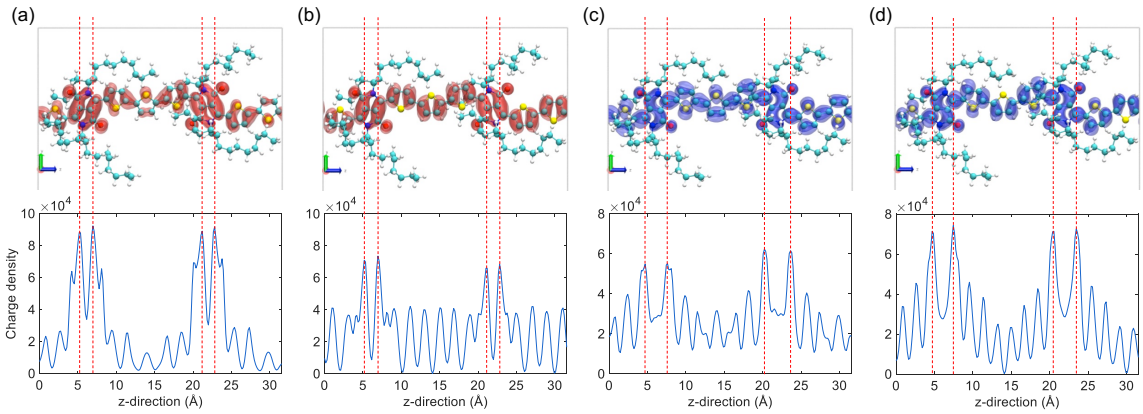

Figure 6. The charge density of the frontier molecular orbitals at the ground state via HSE06 hybrid functionals: **(a)** The orbital of 311, HO-1, **(b)** The orbital of 312, HO, **(c)** The orbital of 313, LU, and **(d)** The orbital of 314, LU+1. Shaded areas indicate the electron density. To plot the isosurfaces, an isovalue of 0.002 is used.

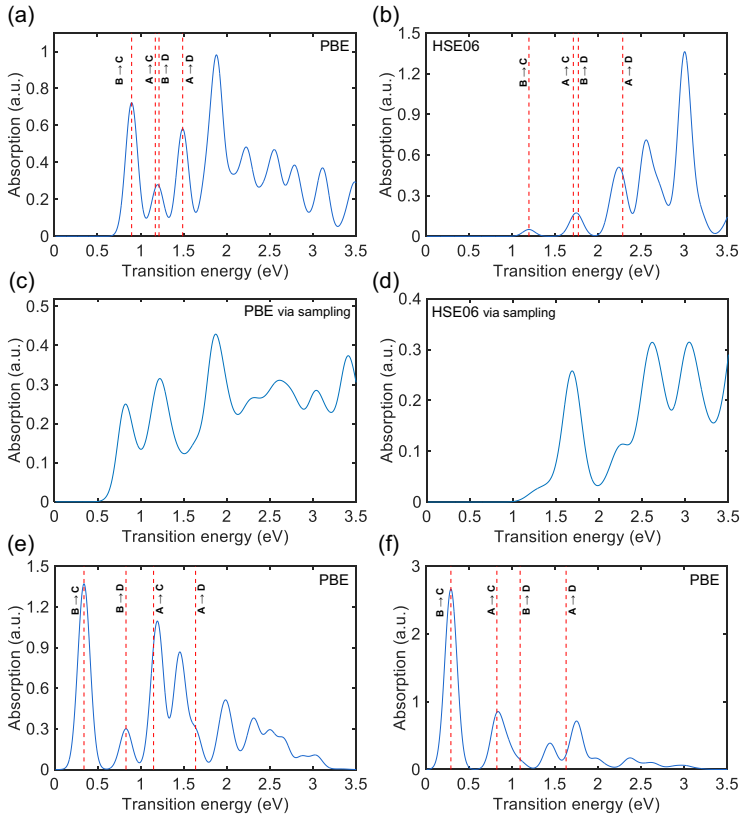

Figure 7. (a) Absorption spectra of CP model using PBE exchange-correlation functional. Dashed lines show the transition energy between selected orbitals where the lowest energy is predicted for the transition from HOMO to LUMO (B to C). Four frontier orbitals near the band gap are labeled. **(b)** Absorption spectra vs. transition energy of the CP model calculated using the HSE06 functional. **(d)** Absorption spectra vs. transition energy graph for the reference model using PBE functional with *k*-point sampling of 16 *k*-points. **(d)** Absorption spectra vs. transition energy graph for the same model using HSE06 functional with *k*-point sampling of 16 *k*-points. **(e)** Absorption spectra vs. transition energy graph of the CP model in case of injected electron doping (n-type doping, negative polaron). Dashed lines show the transition energy between selected orbitals where the lowest energy is predicted for the transition from HOMO to LUMO (B to C). **(f)**

Absorption spectra vs. transition energy graph for the CP model in case of injected hole doping (p-type doping, positive polaron).

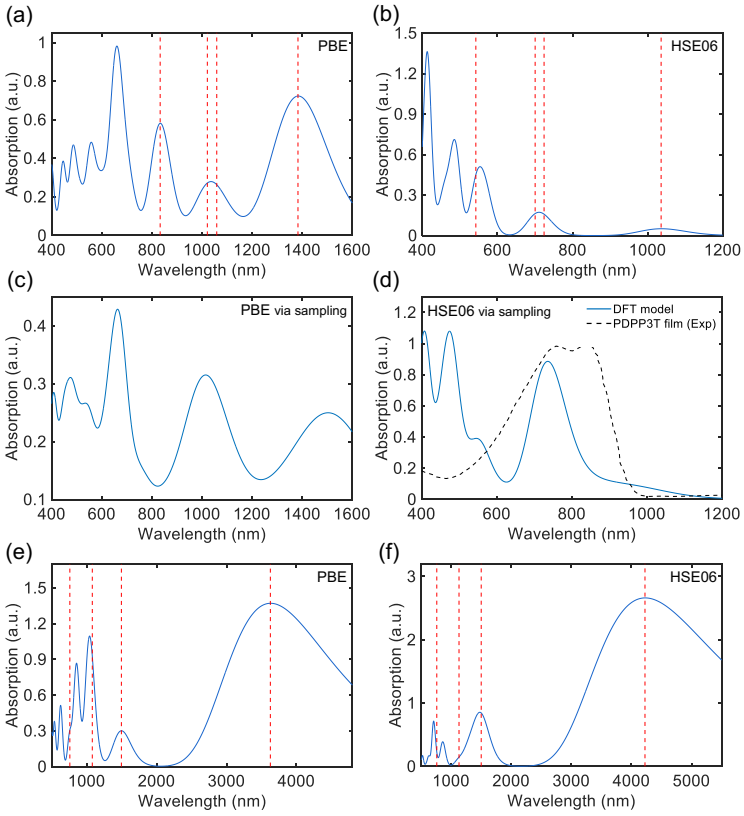

Figure 8. (a) Absorption spectra vs. wavelength graph of the CP model via PBE exchange-correlation functional. **(b)** Absorption spectra vs. wavelength plot for the CP model using HSE06 functional. **(c)** Absorption spectra vs. wavelength graph of the reference model using PBE functional with 16 *k*-points. **(d)** Absorption spectra vs. wavelength graph of the same model using the HSE06 functional with 16 *k*-points. The experimental results of the current polymer are indicated in black dashed line.[85] **(e)** Absorption spectra vs. wavelength of the CP model in case of injected electron doping (n-type, negative polaron). **(f)** Absorption spectra vs. wavelength graph of the CP model in case of injected hole doping (p-type, positive polaron).

- **TOC Graphic:**

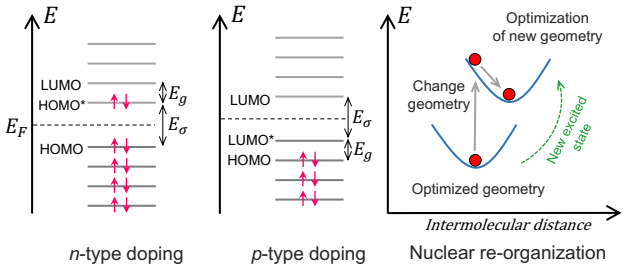
E
LUMO
HOMO*
HOMO
E_F
E_g
E_σ
n-type doping
E
LUMO
LUMO*
HOMO
E_σ
E_g
p-type doping
E
Optimization of new geometry
Change geometry
New excited state
Optimized geometry
Intermolecular distance
Nuclear re-organization